Structural and Magnetic Dynamics of a Laser Induced Phase Transition in FeRh

S. O. Mariager, F. Pressacco, G. Ingold, A. Caviezel, E. Möhr-Vorobeva, P. Beaud, S. L. Johnson, C. J. Milne, E. Mancini, S. Moyerman, E. E. Fullerton, R. Feidenhans'l, C. H. Back, and C. Quitmann

Structural and magnetic dynamics of a laser induced phase transition in FeRh

S. O. Mariager,[1, *] F. Pressacco,[2] G. Ingold,[1] A. Caviezel,[1] E. Möhr-Vorobeva,[1] P. Beaud,[1] S. L. Johnson,[1] C. J. Milne,[3] E. Mancini,[2] S. Moyerman,[4] E. E. Fullerton,[4] R. Feidenhans'l,[5] C. H. Back,[2] and C. Quitmann[1]

[1]*Swiss Light Source, Paul Scherrer Institut, 5232 Villigen, Switzerland*
[2]*Fakultät für Physik, University of Regensburg, 93053 Regensburg, Germany*
[3]*École Polytechnique Fed Lausanne, 1015 Lausanne, Switzerland*
[4]*University of California, San Diego, La Jolla, CA 92093-0401, USA*
[5]*Niels Bohr Institute, University of Copenhagen, 2100 København, Denmark*

We use time-resolved x-ray diffraction and magnetic optical Kerr effect to study the laser induced antiferromagnetic to ferromagnetic phase transition in FeRh. The structural response is given by the nucleation of independent ferromagnetic domains ($\tau_1 \sim 30$ps). This is significantly faster than the magnetic response ($\tau_2 \sim 60$ps) given by the subsequent domain realignment. X-ray diffraction shows that the two phases co-exist on short time-scales and that the phase transition is limited by the speed of sound. A nucleation model describing both the structural and magnetic dynamics is presented.

To date the fastest manipulation of magnetic films and elements are induced by single fs laser pulses and include domain switching and demagnetization on sub-ps time-scales [1–4]. On similar time scales magnetization has been switched by ultrashort but strong magnetic field pulses generated by relativistic electron bunches [5] and stripline techniques [6], while a third intriguing option is the manipulation of the magnetic energy landscape by strong single cycle electric field pulses [7]. Generation of a magnetic moment is equally interesting but harder to achieve on an ultrafast timescale. Ferromagnetic (FM) order can be established in ordinary FM materials by cooling from the paramagnetic phase, but the process is limited by heat transfer and typical timescales are nanoseconds. In this context the antiferromagnetic (AFM) to FM phase transition in FeRh ($T_T \approx 375K$) is interesting because it can be induced by fs laser pulses. The first order phase transition from the low temperature AFM phase is accompanied by a ∼0.5 % volume increase, and though this has been known since 1939 [8] the physical mechanism behind the transition has never been resolved and is still debated [9–11].

The ultrafast transition has been studied in all-optical pump-probe experiments using both transient reflectivity and time resolved magneto optical Kerr effect (TR-MOKE) [12, 13]. While the reflectivity measures a combination of electronic and structural properties, TR-MOKE measures the magnetization. In addition x-ray magnetic circular dichroism (XMCD), which is element specific, has been used to probe the transition [14]. This study found a gradual growth of the magnetization on a time-scale of ∼ 100 ps. In none of these experiments was a separate determination of the lattice dynamics possible. The magnetization dynamics have been simulated with the Landau-Lifshitz-Gilbert equation and a model which considers growth of a non-homogenous magnetization proportional to the spin-temperature followed by a slower alignment and precession of the local magnetic moments [15].

In order to unravel the physical processes underlying the phase transition a prerequisite is the ability to distinguish the contributions arising from the lattice- and magnetic- dynamics. In this letter we report a time resolved x-ray diffraction (XRD) experiment directly measuring the structural dynamics and providing the evolution of the AFM and FM volume fractions with a time resolution of ~ 200 fs. The results are combined with TR-MOKE measurements on the same sample and are explained using a simple model describing the nucleation and subsequent alignment of FM domains.

The FeRh epitaxial thin film ($d = 47$ nm) was grown on MgO(001) by co-magnetron sputtering from elemental targets. The film is epitaxial with a (001) surface. Upon heating through the phase transition the lattice expands 0.7 % along the surface normal, in contrast to the isotropic expansion of bulk samples, indicating a strong in-plane strain.

The time-resolved XRD was performed at an x-ray energy of 7 keV using a synchrotron slicing source (200 ph/pulse at 2 kHz and 1.2 %bw) as probe and an 800 nm 120 fs p-polarized laser pulse with an incidence angle of 12° as pump, resulting in a total time resolution of 200 fs [16]. The x-ray gracing incidence angle was either $\alpha = 0.51^o$ or 0.71^o, in order to match the penetration depth of the x-ray probe to either the laser pump (penetration depth 15 nm) or to the film thickness (47 nm). Due to the grazing angle the x-ray spot size was 0.4×1 mm^2. The (101) Bragg reflection was recorded with a two dimensional PILATUS 100K pixel detector and rocking curves with 60 discrete images were acquired by rotating the sample around the surface normal ($\pm 2.5^o$) [17].

The TR-MOKE measurements were performed at 72 kHz as a two-color pump-probe experiment with 200 fs cross-polarized 800 nm p-polarized pump and 400 nm probe pulses. The probe (58×26 μm^2) had an incidence angle of 60° with respect to the surface while the pump was incident along the surface normal (90°). We used a
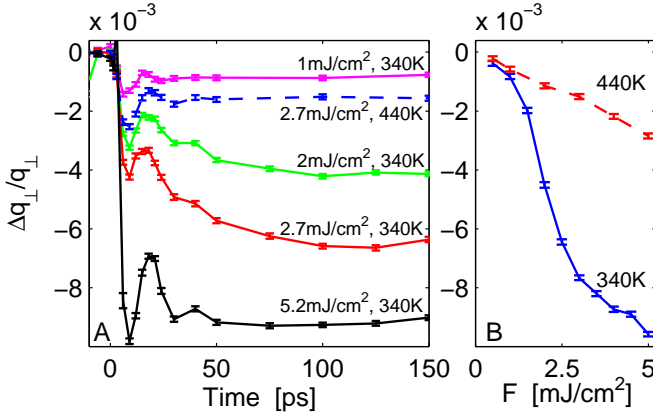
FIG. 1: (Color online) Shift of the center of the (101) Bragg peak after laser excitation. (A) As a function of time delay. (B) As a function of fluence at a fixed time delay of 145 ps for temperatures above and below $T_T = 375K$.
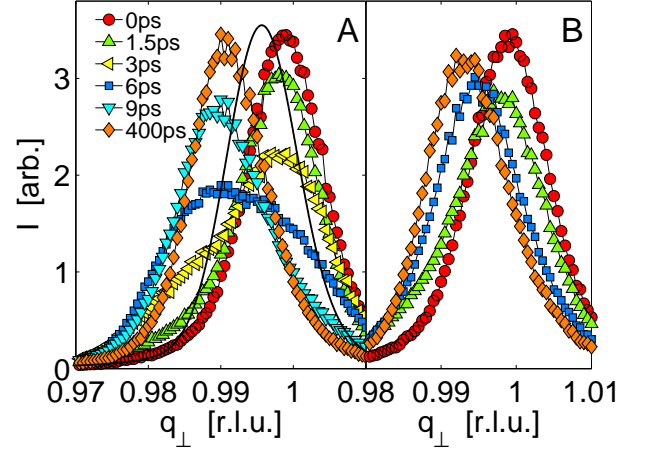

FIG. 2: (Color online) Bragg reflections obtained at different time delays, (A) for a pump fluence of 5.2 mJ/cm^2 and (B) for a pump fluence of 2.7 mJ/cm^2. The solid line is the simulated Bragg reflection at t=6ps under the sole influence of thermal strain.

longitudinal geometry with an applied in-plane external field of 0.1 T. The time dependent traces were recorded for opposite orientations of the external field and the Kerr rotation is the difference of the two traces [18].

In FIG. 1A we show the shift of the center of the Bragg peak as a function of time and laser fluence. As the expansion due to the film geometry is purely one dimensional, the shift occurs along the surface normal ($q_\perp$). A negative peak shift corresponds to an expansion of the lattice, and for a single unstrained phase the peak shift is proportional to the lattice expansion, $\Delta a/a \approx -\Delta q_\perp/q_\perp$. We first consider data obtained at a sample temperature of $T = 340$ K $<$ T$_T$. At a pump fluence of 1 mJ/cm^2 the Bragg peak shifts to a new equilibrium position through a single damped oscillation. This is the signature of a thermally induced strain wave [19] and the period $T=$ 18.6$\pm$0.9 ps (95% confidence interval) is given by the time it takes a strain wave to travel back and forth through the film, $T = 2d/v$. The resulting speed of sound $v =$ 5.1 km/s is consistent with the literature [20]. At higher pump fluences the strain wave is still present but accompanied by an increased peak shift. At intermediate (2-2.7 mJ/cm^2) laser fluences this extra peak shift is slower than the strain wave, while at high laser fluences (5.2 mJ/cm^2) the time scales are comparable. We attribute this peak shift to the transformation from the AFM to the FM phase, and since the peak shift at intermediate fluences is slower than the strain wave, the strain wave can not be the driving force of the transition. In FIG. 1B the peak shift is shown as a function of fluence for a time delay of 145 ps. A deviation from the linear fluence dependence given by thermal expansion, is observed above 1 mJ/cm^2. This threshold behavior is the signature of a laser-induced phase transition. The threshold fluence of $\sim$1 mJ/cm^2 corresponds to a temperature increase of 32 K [25]. This matches the difference

between the sample (340 K) and the transition temperature (T$_T$=375 K) and is consistent with the thermal nature of the laser induced transition. As a final verification that the peak shift arises from the AFM to FM phase transition the sample was heated to 440 K, well above T$_T$. At this temperature the peak shift is given solely by thermal expansion. We thus unambiguously confirm the laser induced AFM to FM phase transition.

In FIG. 2A we further show the full Bragg peaks for several time delays and a fixed pump fluence of 5.2 mJ/cm^2. At $t = 0$ ps the entire film is in the AFM phase. At $t = 400$ ps the entire film has been driven into the FM phase. The full transformation is evident as the two peaks have the same shape. At intermediate times the peak is a sum of the two distinct peaks corresponding to the two phases. We thus directly confirm the coexistence of the two structural phases at short time scales. This is supported by the solid line which is the calculated Bragg peak at $t = 6$ ps under the sole influence of thermal strain [19]. It is thus evident that the transition proceeds through the decrease of the AFM phase and increase of the FM phase, rather than through a continuous change of the lattice constant. The phase coexistence is a common trait of first order transitions and has been observed statically in FeRh for both the magnetic [14] and the crystallographic structure [21]. FIG. 2B shows similar Bragg peaks obtained at a fixed pump fluence of 2.7 mJ/cm^2. In this case the final state ($t = 400$ps) consists of both AFM and FM structure.

In FIG. 1A it can be seen that the amplitude of the initial strain wave does not scale with fluence above the threshold. Thus the phase transition adds to the magnitude of the strain wave. The fact that the phase of the FM peak is initially strained is also seen in FIG. 2A.

Since the stress is relaxed at the speed of sound at least for parts of the film the underlying change in energy landscape from AFM to FM appears faster than $\tau \sim d/v$. This timescale is the limit for the structural transition.

To obtain a quantitative measure of the structural change due to the phase transition we separate it from the effects of the strain wave. In our experiment the grazing incidence geometry and the relatively low x-ray energy limit the separation $\Delta q_\perp$ between the AFM and FM peaks, but the two contributions can be systematically extracted from the measured data by fitting it to the sum of two symmetric functions $(a/\cosh((x-b)/c)^2)$ [26]. One such fit is shown in the insert in FIG. 3A. This way the integrated intensities which are proportional to the scattering volumes of the two phases can be extracted, and in FIG. 3A the volume fraction of the FM phase (V_{FM}) is shown as a function of time delay. Before the arrival of the laser pump the film is entirely in the AFM phase and $V_{FM}=0$. After laser excitation the FM volume grows to saturation within 100 - 200 ps. Increasing the fluence from 2.0 to 2.7mJ/cm^2 increases the transformed volume fraction of the FM phase V_{FM}^* from 32% to 59%. By decreasing the x-ray penetration depth from 47 nm $(\alpha = 0.71^o)$ to 15 nm (0.51^o) we see that for smaller probe depths V_{FM} rises significantly faster, while the transformed volume is only increased slightly. This implies that the nucleation of the FM phase starts at the free surface while the final phase consists mainly of domains penetrating the entire film depth.

To compare the change in structure to the change in magnetization we measured the change in Kerr rotation $(\Delta\Theta_{kerr})$ on the same sample but at 313 K, as shown in FIG. 3B. The higher pump fluences applied compensate for the lower sample temperature. As for the x-ray data we observe a threshold in laser fluence. Below the threshold there is no change in magnetic moment (1.3 mJ/cm^2) while above the threshold the Kerr rotation increases and reaches saturation after several hundred ps (3.1 and 4.5 mJ/cm^2). For the first 100 ps the dynamics appears to follow a power law, in strong contrast to the growth of V_{FM}. As shown in the model below this difference arises because XRD measures the volume of FM domains, while TR-MOKE measures their alignment. Our TR-MOKE results are in agreement with previous XMCD [14] and TR-MOKE [12, 13] experiments, except for the previously reported ultrafast TR-MOKE component which we do not observe. The absence of the ultrafast response may have two reasons. First, TR-MOKE is prone to optical artifacts in the first hundreds of fs after excitation. Second, the absence might be due to the different probe spot size used in the different experiments, as this determines whether or not the magnetization is averaged over many FM domains or just a few.

We now present a model describing the observed dynamics in terms of nucleation and alignment of FM domains. We assume that the film is instantaneously heated
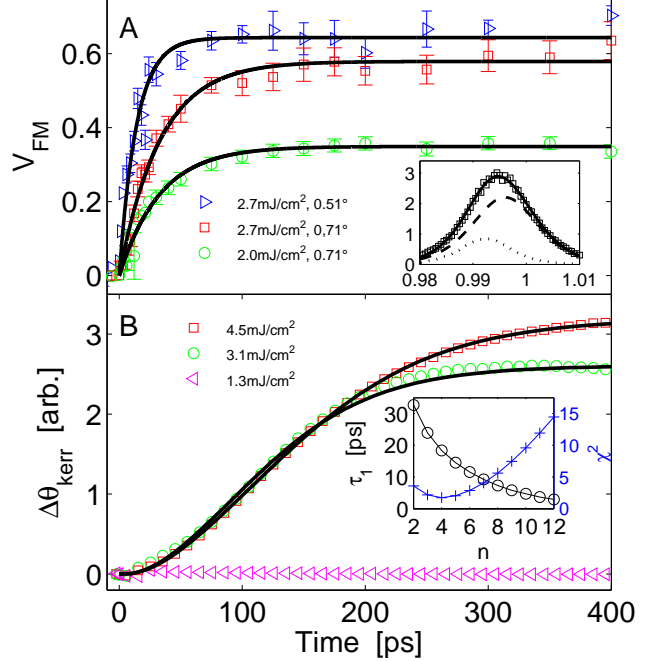

FIG. 3: (Color online) (A) Evolution of the volume fraction of the expanded FM phase as a function of time delay, shown for two different pump fluences and incidence angles. The insert illustrates the fitting procedure (t = 6ps, 2.7 mJ/cm^2), showing the AFM (dashed) and FM (dotted) fit functions, and their sum (solid). (B) Transient Kerr rotation for comparable fluences. The inset shows the dependence of the time constant τ_1 (o) and a chi-square estimator (+) on the model parameter n. The solid lines are fits to the data as described in the text.

above T_T and that the nucleation of the FM phase proceeds through nucleation at many independent sites. The rate of change of V_{FM} is then proportional to V_{AFM} and described by a single time constant τ_1 which may differ for the structural and magnetic changes. Because the transition is of first order the final state may be mixed. To account for this we introduce the final fraction of FM phase V_{FM}^*. As $V_{FM} + V_{AFM} = 1$ we then find:

$$\frac{dV_{FM}}{dt} = \frac{V_{AFM} - (1 - V_{FM}^*)}{\tau_1} = \frac{V_{FM}^* - V_{FM}}{\tau_1} \qquad (1)$$

This is essentially the Avrami model without growth of existing domains [22] and the solution is the exponential function $V_{FM}^*(1 - \exp(-t/\tau_1))$. The depth dependence is only included by allowing different time constants when averaging across different probe depths. This exponential function has been used to fit the data in FIG. 3A and describes the data very well. Within error bars we find the same time constant $\tau_1 = 33 \pm 4$ ps for both intermediate fluences, while $\tau_1 = 14 \pm 3$ ps at $\alpha = 0.51^o$. The exponential growth of V_{FM} is only observed when the nucleation of independent domains is dominant while the growth of

existing domains is suppressed. As the x-ray spot size is 0.4×1 mm^2 the distance between nucleation sites must then be less than ~ 10 μm.

In order to describe the magnetization we assume that the FM domains nucleate with the magnetization fixed into one of n directions and that all n directions are equally probable. We assume one of these directions is favored by the applied magnetic field and define the volume fraction V_A of FM phase aligned to the applied field and the volume fraction V_n not yet aligned. These satisfy $V_{FM} = V_n + V_A$. We finally assume that alignment of the magnetization occurs by growth of the aligned FM domains at the expense of non-aligned FM domains, as described by a product term $V_A V_n/\tau_2$ and a single time-constant τ_2. As this model depends on the existence of both aligned and un-aligned FM domains it supports a theory where short-range interactions are responsible for aligning neighboring FM domains through domain wall motion. Given these assumptions the time evolutions of V_n and V_A are described by two differential equations:

$$\frac{dV_n}{dt} = \frac{n-1}{n}\frac{dV_{FM}}{dt} - \frac{V_A V_n}{\tau_2} \qquad (2)$$

$$\frac{dV_A}{dt} = \frac{1}{n}\frac{dV_{FM}}{dt} + \frac{V_A V_n}{\tau_2} \qquad (3)$$

The MOKE signal is proportional to the magnetization along the preferred direction: $<\mathbf{m}> \propto V_A - V_n/(n\text{-}1)$. This is valid when one of the n-1 directions is opposite to the applied field and the magnetization of the remaining n-2 directions averages to zero. The underlying assumptions of nucleation and coexistence of phases in this model differ from the work by Bergman et al. [15] who assumed that the local magnetization grows monotonously with spin-temperature throughout the film.

The three differential equations are solved numerically for integer values of n, and the result of fitting the result to the TR-MOKE data is shown in FIG. 3B for n=4, which optimizes the fit. The agreement between experiment and fit is excellent with $\chi^2 = 1.8$. The result n=4 is consistent with the in-plane magnetization expected for a cubic thin film, and has been confirmed by static XMCD PEEM images obtained for the same film. For the nucleation time $\tau_1 = 17.8 \pm 0.9$ ps we find, as for the XRD data, the same value for both pump fluences within errorbars. Since the probe depth for the laser in the TR-MOKE experiment is $\sim$11 nm this must be compared to the 14 ± 3 ps obtained with XRD at $\alpha = 0.51^o$. We thus conclude that the timescales of nucleation for magnetic and structural domains are the same within the errorbars. For the final parameter τ_2 which describes the alignment of domains we obtain 72 ± 1 ps and 57 ± 1 ps for fluences of 4.5 mJ/cm^2 and 3.1 mJ/cm^2 respectively. Based on the good agreement between data and model we conclude that the FM domains initially nucleate with un-aligned

moments which are subsequently aligned. We speculate that the initial domain structure is given by the underlying AFM phase and that the mechanism responsible for the re-alignment process is domain wall motion.

The simplest alternative model would describe realignment as a rotation of the total moment of a domain. The realignment term in (2) and (3) would then be $\mp V_n/\tau_2$, independent of V_A. For this model $\chi^2 \approx 30$ which is significantly worse than $\chi^2 = 1.8$ obtained above. In addition the fit is independent of n and results in different nucleation times τ_1 for structure and magnetism. This would imply that the phase transition is independent of the anisotropy and that the magnetic domains nucleate slower than the structure. Both conclusions appear less likely than those reached from (1) - (3). We thus reject the alternative explanation.

In summary we have measured the structural and magnetization dynamics of the AFM to FM phase transition in FeRh on an ultra-fast timescale. XRD allowed us to directly observe the co-existence of the two phases and to derive a simple model which describes the evolution of both the structure and the magnetization. We find two intrinsic timescales: One for the initial nucleation of FM domains which is the same for both magnetic and structural dynamics, and a second for the subsequent growth of FM domains aligned to the applied magnetic field. The co-existence of FM and AFM domains is clearly seen in the XRD data. At intermediate pump fluences the phase transition to a large extent proceeds similarly to static heating, while at higher fluences the structural change is limited by the speed of sound. This speed limit on structural change in principal allows for a significantly faster magnetic response, which we do not observe. It thus appears that magnetic and structural nucleation go hand in hand rather than one driving the other. While the microscopic nature of the magnetization change has been considered theoretically [11], a more definitive answer will require the use of spatially resolved magnetic probes in order not to average the dynamics over many domains.

* Electronic address: `simon.mariager@psi.ch`

[1] E. Beaurepaire, J.-C. Merle, A. Daunois, and J.-Y. Bigot, Phys. Rev. Lett. **76**, 4250 (1996).

[2] C. D. Stanciu, F. Hansteen, A. V. Kimel, A. Kirilyuk, A. Tsukamoto, A. Itoh, and T. Rasing, Phys. Rev. Lett. **99**, 047601 (2007).

[3] I. Radu, K. Vahaplar, C. Stamm, T. Kachel, N. Pontius, H. A. Duerr, T. A. Ostler, J. Barker, R. F. L. Evans, R. W. Chantrell, et al., Nature **472**, 205 (2011).

[4] A. Kirilyuk, A. V. Kimel, and T. Rasing, Rev. Mod. Phys. **82**, 2731 (2010).

[5] C. H. Back, R. Allenspach, W. Weber, S. S. P. Parkin, D. Weller, E. L. Garwin, and H. C. Siegmann, Science **285**, 864 (1999).

[6] T. Gerrits, H. van den Berg, J. Hohlfeld, L. Bar, and T. Rasing, Nature **418**, 509 (2002).

[7] S. J. Gamble, M. H. Burkhardt, A. Kashuba, R. Allenspach, S. S. P. Parkin, H. C. Siegmann, and J. Stohr, Phys. Rev. Lett. **102**, 217201 (2009).

[8] M. Fallot and R. Hocart, Rev. Sci. **77**, 498 (1939).

[9] V. L. Moruzzi and P. M. Marcus, Phys. Rev. B **46**, 2864 (1992).

[10] R. Y. Gu and V. P. Antropov, Phys. Rev. B **72**, 012403 (2005).

[11] L. M. Sandratskii and P. Mavropoulos, Phys. Rev. B **83**, 174408 (2011).

[12] J. U. Thiele, M. Buess, and C. H. Back, Appl. Phys. Lett. **85**, 2857 (2004).

[13] G. P. Ju, J. Hohlfeld, B. Bergman, R. J. M. van de Veerdonk, O. N. Mryasov, J. Y. Kim, X. W. Wu, D. Weller, and B. Koopmans, Phys. Rev. Lett. **93**, 197403 (2004).

[14] I. Radu, C. Stamm, N. Pontius, T. Kachel, P. Ramm, J.-U. Thiele, H. A. Dürr, and C. H. Back, Phys. Rev. B **81**, 104415 (2010).

[15] B. Bergman, G. Ju, J. Hohlfeld, R. J. M. van de Veerdonk, J.-Y. Kim, X. Wu, D. Weller, and B. Koopmans, Phys. Rev. B **73**, 060407 (2006).

[16] P. Beaud, S. L. Johnson, A. Streun, R. Abela, D. Abramsohn, D. Grolimund, F. Krasniqi, T. Schmidt, V. Schlott, and G. Ingold, Phys. Rev. Lett. **99**, 174801 (2007).

[17] S. O. Mariager, S. L. Lauridsen, A. Dohn, N. Bovet, C. B. Sorensen, C. M. Schlepuetz, P. R. Willmott, and R. Feidenhans'l, J. Appl. Cryst. **42**, 369 (2009).

[18] B. Koopmans, in *Spin dynamics in confined magnetic structures II* (Springer, 2003).

[19] C. Thomsen, H. T. Grahn, H. J. Maris, and J. Tauc, Phys. Rev. B **34**, 4129 (1986).

[20] J. A. Ricodeau and D. Melville, J. Phys. F - Metal phys. **2**, 337 (1972).

[21] J. W. Kim, P. J. Ryan, Y. Ding, L. H. Lewis, M. Ali, C. J. Kinane, B. J. Hickey, C. H. Marrows, and D. A. Arena, Appl. Phys. Lett. **95**, 222515 (2009).

[22] M. Avrami, J. Chem. Phys. **7**, 1103 (1939).

[23] J. Y. Rhee and D. W. Lynch, Phys. Rev. B **51**, 1926 (1995).

[24] M. P. Annaorazov, K. A. Asatryan, G. Myalikgulyev, S. A. Nikitin, A. M. Tishin, and A. L. Tyurin, Cryogenics **32**, 867 (1992).

[25] Calculated with reflectivity R = 0.32, penetration depth = 11 nm [23], density 9.88 g/cm^3 and specific heat capacity 465 J/kgK [24].

[26] To obtain the fit the AFM Bragg peak position was fixed to the peak shift measured at 1 mJ/cm^2 but scaled with fluence. At intermediate fluences, where the timescales of the phase transition and the strain wave differ significantly, the FM Bragg peak was restricted by an upper limit given by the measured peak shift at 400 K. To fix the FM peak position at $\alpha = 0.51^o$ the shift obtained from the scaled strain wave was superimposed on the upper limit.